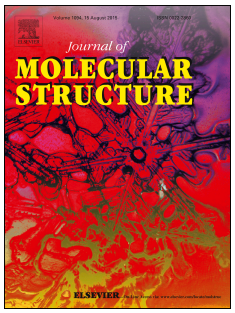

Chelating behavior of 3-amino-4,6-dimethyl-1*H*-pyrazolo[3,4-b]pyridine ligand towards some metal ions, spectral and thermal measurements as well as molecular modeling and biological studies

Mamdouh S. Masoud, Saeyda A. AbouEl-Enein, Alaa E. Ali, Eman H. Abd Elhamed

PII: S0022-2860(19)31281-5

DOI: https://doi.org/10.1016/j.molstruc.2019.127172

Reference: MOLSTR 127172

To appear in: *Journal of Molecular Structure*

Received Date: 18 June 2019

Revised Date: 29 September 2019

Accepted Date: 1 October 2019

Please cite this article as: M.S. Masoud, S.A. AbouEl-Enein, A.E. Ali, E.H. Abd Elhamed, Chelating behavior of 3-amino-4,6-dimethyl-1*H*-pyrazolo[3,4-b]pyridine ligand towards some metal ions, spectral and thermal measurements as well as molecular modeling and biological studies, *Journal of Molecular Structure* (2019), doi: https://doi.org/10.1016/j.molstruc.2019.127172.

Chelating behavior of 4, 6-dimethyl-1H-pyrazolo [3, 4-b] pyridine-3-amine ligand towards some metal ions, spectral, thermal and molecular modeling measurements as well as biological studies

Mamdouh S. Masoud[a], Saeyda A. AbouEl-Enein[b]*, Alaa E. Aly[c], Eman H. Abd Elhamed

[a] Chemistry Departmen, Faculty of Science, Alexandria University, Egypt
[b]Chemistry Department, Faculty of Science, Menoufia University, Egypt
[c]Chemistry DepartmenFaculty of Science, Damnhour University, Egypt

Graphical abstract

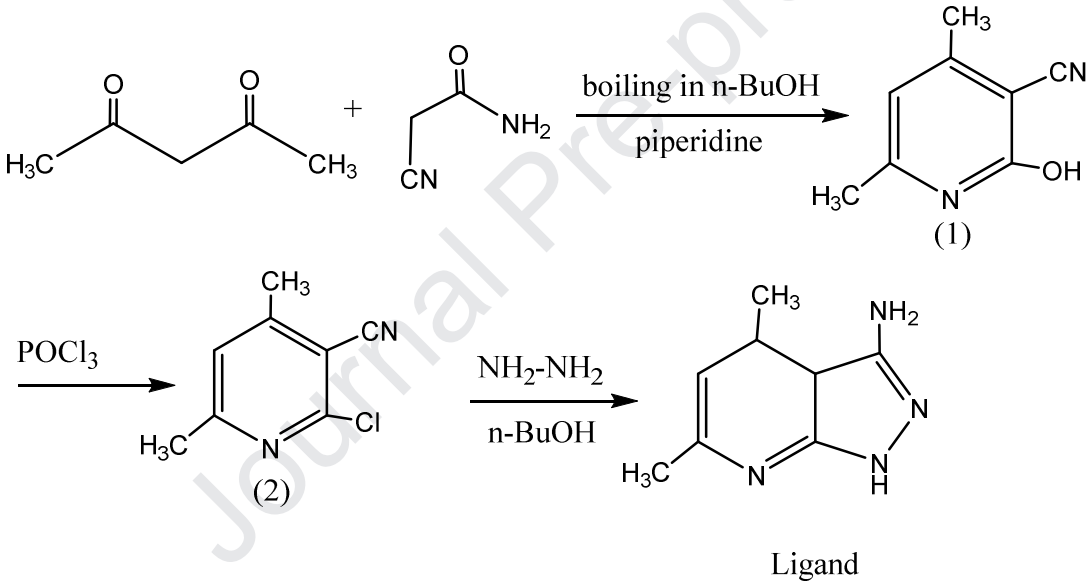

Chelating behavior of 3-amino-4,6-dimethyl-1*H*-pyrazolo[3,4-b]pyridine ligand towards some metal ions, spectral and thermal measurements as well as molecular modeling and biological studies

Mamdouh S. Masoud[a], Saeyda A. AbouEl-Enein[b]*, Alaa E. Ali[c], Eman H. Abd Elhamed

[a] Chemistry Departmen, Faculty of Science, Alexandria University, Egypt
[b]Chemistry Department, Faculty of Science, Menoufia University, Egypt
[c]Chemistry Department, Faculty of Science, Damnhour University, Egypt

Abstract

The 3-amino-4,6-dimethyl-1*H*-pyrazolo[3,4-b]pyridine ligand and its Mn(II), Pd(II), Fe(III), Cr(III), Ru(III), Hf(IV), Zr(IV) and UO_2(II) metal complexes were synthesized and characterized by means of elemental analysis, spectral studies and thermal investigation. Also, the theoretical studies that done by Spartan '14 V1.1.4 software supported the experimental studies. The infrared data suggest that the ligand coordinates to the metal ions as a neutral monodentate moiety through nitrogen atom of amino group. The complexes are formed with 1:2 and 1:3 (M:L) molar ratios. All complexes possesses octahedral geometry except the Pd(II) complex that presents a square planar geometry. Thermal analyses (TGA and DTG) of ligand and its metal complexes are performed in order to identify the external solvents molecules and thermal stability ranges of the complexes. The X- ray diffraction studies suggest orthorhombic structure of P type lattice for Pd(II) complex and monoclinic structure of P type lattice for Cr(III) and Zr(IV). Theoretical calculations are performed to corroborate the experimental results. Some theoretical parameters are reported in order to compare the reactivity of the compounds. The cytotoxic activity of the ligand and its Pd(II) and Ru(III) complexes is evaluated against breast MCF-7 cell line. Pd(II) complex presents a higher activity. The synthesized ligand and its Pd(II), Cr(III) and Zr(IV) metal complexes also are screened for antibacterial activity. The ligand and its tested complexes has weak activity towards a Gram-positive bacteria and no activity towards Gram-negative bacteria except Pd(II) complex.

Keywords*: Pyrazolopyridine complexes; Thermal studies; Cytotoxic activity.*

*Correspondence author: dr.saeyda_elenein@yahoo.com

1. Introduction

Pyrazol and pyridine rings are fused to give different pyrazolopyridine ring systems [1]. 4,6-dimethy-l-1H-pyrazolo[3,4-b]pyridine-3-amine is the most important pyrazolopyridine derivative that is used as versatile precursor to prepare several heterocyclic derivatives (fluorescence dyes, Schiff base, hydrazide and etc…..). A number of heterocyclic compounds containing pyrazolopyridine systems have been associated with several pronounced medicinal and biological activities as anxiolytic, antiviral and anti-inflammatory agents [2-9]. Also, in coordination chemistry, pyrazolopyridine derivatives can be used as ligands coordinating to metals in the different ways. The amidine moiety (-N=CH-NH_2) of these molecules is a favorable site of coordination found in some metallic complexes with biological applications. Also, their transition metal complexes have different applications and are used for anticorrosion protection of stainless steel in aggressive media [10].

Along with transition metals, inner transition metals can offer remarkable physico-chemical properties and have applications both in the technological field (sensor devices, optical fibers, lasers, *etc*.) and in the medical field (in diagnosis and therapy). The potential of inner metal complexes for this type of applications is mainly dependent on the metal center, chromophore and on the nature of the ligands [11,12]

The present work explores experimentally and theoretically the coordination behave of 3-amino-4,6-dimethyl-1*H*-pyrazolo[3,4-b]pyridine towards some transition and inner metal ions. The structure of synthesized metal complexes [(Mn(II), Pd(II), Fe(III), Cr(III), Ru(III), Hf(IV), Zr(IV) and UO_2(II)] is elucidated using elemental analysis, spectral, magnetic, molar conductance measurements and thermogravimetric analysis as well as XRD studies. The cytotoxicity activity of ligand and its Pd(II) and Ru(III) complexes is evaluated against breast MCF-7 cell line also, the antimicrobial activity is done for ligand and its Pd(II), Cr(III) and Zr(IV) metal complexes. The geometry of ligand and its metallic complexes was obtained through Semi-Empirical (PM3) calculations.

2. Experimental

2.1. Materials and Methods

All chemicals are of analytical grade (BDH, Sigma or Aldrich) and are used as received without further purification. Micro analytical data of (C, H, N) are performed on a Perkin Elmer-2400 elemental analyzer at Main Defense Chemical Laboratory, Egypt. Mn(II) and Fe(III) ions are assayed by complexmetric titration [13]. However Pd(II), Ru(III), Hf(IV), Zr(IV), Cr(III) and UO_2(II) ions are evaluated by gravimetric analysis. The chloride ions are estimated by Mohr's method [13]. Infrared spectra of solid potassium bromide samples are recorded on a Nicolet FT-IR spectrophotometer in the range 4000-400 cm^{-1}. ^1H NMR spectra are measured in DMSO-d^6 on a Varian Gemini 200 NMR spectrophotometer at 300 MHz. The electronic absorption spectra are obtained in Nujol mulls using a Perkin Elmer Lambda 4B spectrophotometer. Molar conductance measurements of metal complexes are determined in DMSO solution (10^{-3} M) at room temperature using a type CD6N Tacussel conductimeter. The thermogravimeteric investigation (TG/DTG) are diagrammed under a heating rate of 10^oC/min, nitrogen atmosphere and a flowing rate of 20 mL/min by using a Shimadzu DAT/TG-50 thermal analyzer. A Johnson Matthey magnetic susceptibility balance using Gouy method at room temperature is employed to measure the magnetic susceptibility values. Diamagnetic corrections are calculated using Pascal's constants [14]. The effective magnetic moments are calculated from $\mu_{eff} = 2.84(X_M^{corrt}\ T)^{1/2}$ equation. Fast Atom Bombardment (FAB) mass spectra for the ligand and some metal complexes are recorded on a Shimadzu Qp-2010 Plus spectrometer at Al-Azhar University, the Regional Center for Mycology and Biotechnology. Powder X-ray diffraction for some complexes are registered by using an X-ray diffractmeter equipped with a graphite monochromator in the range of (2θ = 5-90°) by nickel separated CuKα radiation (λ = 1.54060 A°). The theoretical quantum chemical calculations are done by Spartan '14 V1.1.4 software. The cytotoxicity is carried out at Medicinal Technology Center, Medicinal Research Institute, Alexandria University. However, the antibacterial activity of samples is evaluated in the Regional Center for Mycology and Biotechnology at Al-Azhar University, respectively. Melting points are measured by using Stuart melting point apparatus.

2.2. Preparation of 3-Amino-4,6-dimethyl-1*H*-pyrazolo[3,4-b]pyridine (HL) ligand

The ligand was prepared as reported [15,16]. The cyanoacetamide reacts with acetylacetone in n-butanol on boiling and in presence of a few drops of pipridine to give 2-hydroxy-2,6-dimethylpyridine-3-carbonitrile (1). The compound (1) was treated with phosphorus oxychloride ($POCl_3$) to give 2-chloro-4,6-dimethylpyriine-3-carbonitrile (2). The compound (2) was reacted with hydrazine hydrate in boiled n-butanol to give 3-amino-4,6-dimethyl-1*H*-pyrazolo[3,4-b]pyridine. The melting point of the product is 273°C. The reactions steps for synthesis of 3-amino-4,6-dimethyl-1*H*-pyrazolo[3,4-b]pyridine are shown in Scheme1

Insert Scheme 1 and its caption here

2.3. Preparation of metal complexes

The complexes are prepared by adding an ethanolic solution of appropriate metal chloride salts (Mn(II), Pd(II), Fe(III), Cr(III), Ru(III), Hf(IV), Zr(IV)) and UO_2(II) nitrate to an ethanolic suspension solution of ligand with molar ratio (1M:2L). The reaction mixture is refluxed for hours with magnetically stirring. The products are cooled, filtered off, washed several times with ethanol and dried in vacuum desiccator over anhydrous $CaCl_2$. The melting points of all complexes are higher than 360°C

2.4. Biological Activity

2.4.1. Antitumor Activity

The MTT (3-(4,5-dimethylthiazol-2-yl)-2.5-diphenyltetrazolium bromide) assay is a colorimetric method which was used to measure the viable cells without the need for counting the viable cells [17,18]. This method is based on changing the yellow MTT salt to insoluble purple Formazan using active cell line (MCF-7). This assay is utilized to measure the in *vitro* cytotoxicity or cytostatic activity of drugs on cell lines. Evaluation of cytotoxicity of HL ligand and some of its metal complexes **(**Pd(II) and Ru(III)) was tested against breast MCF-7 cell line. These cell lines are cultured in (75 cm^2) culture flasks using Dulbecco's modified Eagle's medium (DMEM) supplemented with 10% (v/v) fetal bovine serum (FBS). Then $3x10^3$ cells/well are maintained and incubated at 37°C for 48h in a moist atmosphere containing 5% CO_2. The growth medium must be changed every other day until the use of cell lines. The test compounds and a positive control compound (doxorubicin) are dissolved in dimethyl sulfoxide (DMSO) and then diluted with H_2O to prepare a series of concentrations (1.562, 3.125, 6.25, 12.50, 25.0, 50.0 and 100 μg/mL). The cells were washed twice and treated with each concentrations of the test compounds and re-incubated for 48h. Then cytotoxicity is determined

using MTT assay. 20μL of MTT solution (5mg/mL) in PBS (phosphate-buffered saline) together with 200 μL of freshly complete media are added to each well and re-incubated for four hours at 37°C. Following the incubation process, the medium is removed and the insoluble purple Formazan crystals have been formed in each well. Then, 100 mL of DMSO solution containing 20 mM HCl is added to each well and re-suspended until the crystals have been dissolved. The optical density is determined at 490 nm using colorimetric method. This experiment is repeated in triplicate [19]. The quantity of the colored product is directly proportional to the number of live cells in the culture. The results are expressed as IC_{50} (a dose of compound that inhibits cell growth by 50%) which is calculated from cell viability percent.

$$\text{Cell Viability\%} = \frac{\text{OD (Optical density)of sample well}}{\text{OD (Optical density)in controll well}} \times 100$$

2.4.2. Antimicrobial Activity

Antimicrobial activity is done on (**HL**) ligand and some of its metal complexes against two positive bacteria (*Staphylococcus aureus and Bacillus subtilis*) and two negative bacteria (*Escherchia coli and Pseudomonas aeruginosa*). The antimicrobial activity of the tested compounds is evaluated by means of paper disk diffusion method (9 mm) on Muller Hinton agar [20]. Fresh culture of tested organisms are cleaned using sterile cotton on the surface of prepared Muller Hinton agar. The samples are freshly dissolved in DMSO. 100 μL of prepared samples was loaded separately on paper disk and left until drying. The loaded discs are added to the surface of cultured petri dishes and kept for two hours at 4^{o}C to allow the diffusion of dissolved compounds into agar. The antibiotic control used during assay is Tri-Methoprim/Sulphamethoxazole (SXT) [(1.25/23.75)mcg]. Then the plates are transferred to incubator at 37°C for 24 hrs. After incubation, the diameter of inhibition zone is measured in millimeter (mm) [21].

3. Results and discussion

Characterization of the ligand and its metal complexes

Table 1 represents analytical data of ligand and its metal complexes. The data shows that the ligand coordinated with different metal ions to separate the complexes with 1:2 and 1:3 (M:L) molar ratios. The molar conductance values of investigated complexes are in the range of 5-24 Ω^{-1} cm^2 mol^{-1} indicating the non-electrolytic nature of all complexes and the anions are directly attached to central metal ion in the coordination sphere [21-25]. All the solid metal

complexes are stable, non-hygroscopic and partially soluble in most organic solvents such as chloroform, methanol, ethanol, acetonitrile, DMF and completely soluble in DMSO.

Insert Table 1 and its caption here

3.1. Mass spectra of the ligand and some of its complexes

The FAB spectrum of the ligand (Figure 1) shows accurate parent molecular ion peak at m/z 162 amu, matched with the theoretical molecular weight. The spectrum gives other successive degradation peaks at m/z 147, 132, 117, 104, 90, 76.08, 62 and 48 amu, corresponding to $[C_7H_7N_4]^+$, $[C_6H_4N_4]^+$, $[C_6H_3N_3]^+$, $[C_6H_3N_2]^+$, $[C_6H_3N]^+$, $[C_5H_2N]^+$, $[C_4HN]^+$ and $[C_4]^+$, respectively (Scheme S1).

Results of microanalyses and mass spectra of the complexes 2-8 suggest that their molecular formula are $[Pd(HL)_2Cl_2].H_2O.2EtOH$, $[Fe(HL)_3Cl_2(OH)].4.5H_2O.3.75EtOH$, $[Cr(HL)_3Cl_3].3EtOH$, $[Hf(HL)_2Cl_4].4H_2O.1.5EtOH$, $[Zr(HL)_2Cl_4].H_2O.3EtOH$ and $[UO_2(HL)_2(NO_3)_2].H_2O.3EtOH$ by giving the parent molecular ions at m/z 613.21(Calc. 611.87), 887 (Calc. 885.43), 785 (Calc. 783.15), 785 (Calc. 786.36), 714 (Calc. 713.65) and 950 (Calc. 949.05), respectively. Moreover, additional peaks appear due to fragmentation of complexes that result from rupture of different bonds inside the molecules, Figure 1.

Insert Figure 1 and its caption here

3.2. ^{1}HNMR spectra of the ligand and its Pd(II), Hf(IV) and UO_2(II) complexes

The ^{1}H NMR spectrum of ligand reveals singlet signal at 11.70 ppm assignable to (NH) proton [26]. Also, it shows signal characterized to protons of (NH_2) group at 5.05 ppm [27]. The *C*-methyl protons signal appear as a singlet around 2.87-3.53 ppm [8]. The aromatic protons appear at 6.56 ppm. It is easy to detect the mode of bonding of ligand with metal ions by comparing the ^{1}HNMR spectrum of ligand with that of its complexes containing diamagnetic metal ions (Pd(II), Hf(IV), and UO_2(II)). The spectra of complexes display that all signals are shifted to low frequency relative to free ligand. Upon complexation, the NH_2 signal of ligand exhibits shift in the range of 4.18-5.05 ppm relative to free ligand at (5.05 ppm), referring to its participation in chelation. The pyrazolo (NH) group in Pd(II) complex appear as a broad nature due to intra hydrogen bonding of nitrogen atom of pyridine ring (N…..H-N) and also cannot seen in UO_2(II) and Hf(IV) complexes due to the acidic proton on the hetero atom may be interacted or exchanged with the solvent molecules [28]. The methyl and aromatic protons exhibit slightly

shift due to change the environment. The ^{1}HNMR spectral bands and their assignments are listed in Table S1.

3.3. Infrared spectra of (HL) ligand and its metal complexes

The main spectral bands and their assignments of ligand are given in Table S2 and represented by Figure S1. The IR spectrum of ligand displays fundamental spectral bands located at 3397, 3290, 1623, 1312, 1074 and 491 cm^{-1} characterized to $\upsilon_{as}(NH_2)$, $\upsilon_{sy}(NH_2)$, $\delta(NH_2)$, $\upsilon(C\text{-}NH_2)$, (NH_2) rocking overlapped with pyrazol ring breathing and (NH_2) wagging, respectively [29]. Also, the different vibration mode (υ, δ, γ) of NH; υ(C=N) and υ(N-N) of pyrazol ring are characterized by bands at 3190, 3114, 1458, (771,656); 1607 and 1127 cm^{-1}, respectively [30, 31]. The stretching, deformation and bending vibrations modes of C-H of methyl groups are associated with the bands appear at (2971; 2890), 1407 and 826 cm^{-1}, respectively. The spectrum of ligand gives bands at (3040; 1520), 1023 and (615,579) cm^{-1} refer to stretching, breathing and bending of C-H in plane of pyridine ring, respectively [32].

The infrared spectral bands of free ligand are compared with that of its complexes to infer the mode of bonding between ligand and metallic ion. The infrared spectral bands of all complexes, except Ru(III), show that the $\upsilon_{sy}(NH_2)$ and $\delta(NH_2)$ undergo shift towards higher wavenumber by 14-59 and 19-21cm^{-1}, respectively relative to that of free ligand (Table S2). Also, the $\upsilon(C\text{-}NH_2)$ and $\rho(NH_2)$ of the ligand display changes in their shapes and positions indicating the participation of nitrogen atom of amino group in chelation. The infrared spectra of complexes give new band (absent in ligand) appeared in the range of 526-558 cm^{-1} assignable to υ(M-N) [33,34]. The IR spectrum of UO_2(II) complex shows a band at 920 cm^{-1} which is assigned to υ(O=U=O) [35]. Also the appearance of two bands at 1489 and 1288 cm^{-1} assignable to $\nu_{as}(NO_3^-)$, $\nu_{sy}(NO_3^-)$, respectively indicating that NO_3^- group coordinates as a monodentate moiety [36].

Also, the υ(C=N), υ(N-N) of pyrazol ring and pyridine ring bending in and out of plane are associated with very slight shift in their position. This ruled out the non-involvement of the nitrogen atoms of imine, NH and pyridine ring in coordination to metal ion. The observed shift of (υ, δ) of (NH) group and some bands of pyridine ring after complexation assigned to the existence of inter \ intra molecular hydrogen bonding [37].

The above arguments prove that the ligand behaves as a neutral monodentate one and coordinates with metal ions through nitrogen atom of amino group. This was due to (NH_2) group

had higher neucleophilicity than that of (C=N) group. Also, the monodentate character of HL behaves as similar to reported for some multidentate ligand [38].

Insert Table 2 and its caption here

3.4. Magnetic measurements of metal complexes and electronic absorption spectra of (HL) ligand and its metal complexes

The magnetic moment values per metal ion at room temperature and the Nujol mull electronic absorption bands with their assignments for the ligand and its metal complexes are collected in Table S3 and represented in Figure S2.

The spectrum of ligand gives four bands at 330, 360, 415 and 463 nm assigned to π-π* and n-π* transitions, respectively [39,40]. In complexes, the band observed at 463 nm in the spectrum of ligand assigned to n-π* transition suffered a red shift to 465-480 nm due to a combination of LMCT with d-d transitions [41,42].

The spectrum of the Mn(II) complex displays broad strong and weak bands at 480 and 652 nm assigned to $^6A_{1g}\rightarrow{}^4E_g$ (^4D) (υ_3) and $^6A_{1g}\rightarrow{}^4T_{1g}$ (^4G) (υ_1) transitions, respectively. Also, the higher energy band overlapped with LMCT transition. These transitions are conducted to octahedral stereochemistry around Mn(II) ion. The observed low magnetic moment value 1.83 B.M assigned to low-spin octahedral complex [43].

The Pd(II) complex gives electronic spectral bands at 465 and 668 nm in a strong and weak feature, assigned to $^1A_{1g}\rightarrow{}^1E_g(\upsilon_3)$ and $^1A_{1g}\rightarrow{}^1A_{2g}(\upsilon_1)$ transitions, respectively which are relevant to square planar geometry around Pd(II) metal ion [44].

The Fe(III) complex reveals spectral bands at 670 and 748 nm due to $^6A_{1g}\rightarrow{}^4E_g(^4G)$ and $^6A_{1g}\rightarrow{}^4T_{2g}(^4G)$ transitions, concerning to octahedral complex. The observed low magnetic moment value (3.04 B.M) suggests the existence of high-low spin crossover [45]. This occurs in octahedral complexes with between 4 and 7 electrons especially iron can be either high spin or low spin depending on the size strength of the ligand (value of Δ), the two states have similar energies and can coexist in measurable amounts at equilibrium [46]. The observed spectral bands of Cr(III) complex near 480 and 678 nm due to $^4A_{2g}(F)\rightarrow{}^4T_{1g}(p)$ and $^4A_{2g}(F)\rightarrow{}^4T_{2g}(F)$ transitions, respectively indicating octahedral geometry around Cr(III) ion. Also, the magnetic moment value (4.0 B.M) is an evidence octahedral structure [47].

The spectrum of Ru(III) complex gives electronic spectral bands at 671, 755 nm in broad and weak nature characterized to $^2T_{2g}\rightarrow{}^4A_{2g}$ and $^2T_{2g}\rightarrow{}^4A_{1g}$ transitions, respectively. The μ_{eff} 1.78 B.M confirming low spin octahedral complex [48].

Based on elemental analysis and electronic spectra of diamagnetic Zr(IV), Hf(IV) and UO_2(II) points to octahedral geometry.

The infrared spectra and electronic absorption spectral data as well as the magnetic moment values for the metal complexes established the proposed structures as shown in Figure S3.

3.5. Thermal analysis for ligand (HL) and its metal complexes

The thermogravimetric study is used to identify the type of solvents and describe the behavior of thermal decomposition. The thermogram curves and thermoanalytical data of ligand and its metal complexes are collected in Figure S4 and Table 3, respectively.

The TG curve of the ligand displays thermal stability without weight loss up to 164°C, relevant to the absence of solvent. After that, the TG curve shows progressive weight loss 98.29% in 164-400°C range due to complete pyrolysis of ligand. The pyrolytic process take place fastly in one step and associated with strong sharp DTG peak at T_{max} = 282°C leaving carbon residue (0.25 C). The calculated weight losses of ligand is convenient with TG weight loss of molecule as gases at given temperature range [49]. The mechanism pathway of thermal decomposition showed in Scheme 2.

The thermogram of $[Mn(HL)_3Cl_2.(H_2O)].1.5H_2O$ indicates the loses of one mol of hydrated water molecule in the temperature range of 25-181°C with TG weight loss 2.42 %. The thermal decomposition of unhydrous complex achieved in three stages within 181-266, 266-345 and 345-542°C ranges. These stages are characterized by TG weight losses 28.07, 33.35 and 19.97% due to loss of one mol of pyrazolopyridine plus 0.5 mol of chlorine gas, removal of second mol of pyrazolopyridine, 0.5 mol of chlorine gas plus three mols of carbon and evolution of three mol of nitrogen and eight mol of hydrogen gases additional to 2.5 mol of carbon, respectively. The first and the second decomposition stages are associated with two strong sharp DTG peaks with T_{max} = 248 and 302°C, while the third stage shows weak broad DTG peaks at T_{max}= 377 and 428°C, respectively. The DTG pattern (Figure S4) describes the thermolysis of complex took place fastly in the first and second stages with progressive nature and with nearly similar degradation pathway. The thermolysis process ends with formation of $0.5Mn_2O_3$+2.5C as a final thermal decomposition product [50]. The mechanism of thermal decomposition pathway illustrated in Scheme 2.

Insert Scheme 2 and its caption here

The thermograms and thermoanalytical data of the complexes $[Pd(HL)_2Cl_2].H_2O.2EtOH$, $[Cr(HL)_3Cl_3].3EtOH$ and $[Ru(HL)_3Cl_3].9.5EtOH$ reveals that these complexes are decomposed

by nearly similar pathway. The TG patterns show weight losses in the temperature range of 25-202°C due to release of some solvent of crystallization. After that the Pd(II), Cr(III) and Ru(III) complexes start decomposition at 202, 194 and 146°C and ended at 727, 604 and 644°C, respectively. The thermolysis processes are accomplished mainly through two continuous stages. The first decomposition stage characterized by estimated weight losses 29.06, 25.40 and 35.54% within 202-354, 194-308 and 146-378°C, respectively. Those weight losses are equivalent to removal of (0.5 mol of Cl_2), (0.5 mol of Cl_2 +1.5 mol of $C_{(EtOH)}$) and (one mol of Cl_2 + 4 mol of EtOH) additional to decomposition of one mol pyrazolopyridine moiety, respectively. The second thermal decomposition stage of Pd(II), Cr(III) and Ru(III) assigned by an estimated TG weight losses 42.08, 48.74 and 44.61% up to 727, 604 and 644°C, respectively, concerning to complete ligands pyrolysis as well as removal of rest chloride Table 3. The DTG curve of Cr(III) complex gives two sharp peaks with T_{max} = 243 and (380, 508°C), respectively, whereas Pd(II) shows sharp peaks at T_{max} =303 and (392, 456°C). However the Ru(III) displays medium; shoulder and weak peaks at T_{max} =190, 239, 318 and (427, 542 and 614°C) corresponding to first and second decomposition stages, respectively. The DTG curves deduced that the decomposition of Cr(III) complex achieved through two definite clarified processes. However, the Ru(III) complex is decomposed through overlapped or diffused processes, while the first decomposition stage has definite process whereas second stage has overlapped process for Pd(II) complex. All decomposition processes leading to formation of metal oxides namely PdO, (0.5 Cr_2O_3 + 5C) and 0.5 Ru_2O_3 [51,52]. The events of the thermal decomposition pathway of Pd(II) complex is taken as representative example and is suggested as in scheme 3.

Insert Scheme 3 and its caption here

The thermogram pattern of $[Fe(HL)_3Cl_2$ (OH)].4.5H_2O.3.75EtOH shows that the removal of solvents of crystallization is in the temperature range of 25-237°C. This step subdivides into two steps in the temperature ranges of 25-127 and 127-237°C and associated with TG weight losses 6.59 and 20.60% assignable to removal of 1.25 mol of EtOH and 4 mol of H_2O plus 2.5 mol of EtOH, respectively. The low onset temperature of removal of 1.25 EtOH indicating that the solvent is in lattice voids, whereas the rest solvents involves in lattice structure to raise the thermal stability of complex up to 237°C. This step accompanied with weak and medium DTG peak T_{max}=102 and 186°C, respectively. Then the complex starts decomposition through two overlapped continuous stages within temperature range of 237-419°C with T_{max}=300, 332°C and 419-651°C with T_{max}= 480, 577 °C, respectively. These steps characterized by TG weight losses

12.25 and 48.25% due to dechloronation process plus removal of two mol of (CH_3+H_2) and complete pyrolysis of ligand, respectively. The thermal decomposition processes ends with formation of ($0.5Fe_2O_3$ + 2.5C) as final product [53]. (Scheme 4) shows the mechanism of thermal decomposition pathway of $[Fe(HL)_3Cl_2(OH)].4.5H_2O.3.75EtOH$ complex.

Insert Scheme 4 and its caption here

It is obvious from the thermogram patterns that $[Hf(HL)_2Cl_4].4.H_2O.1.5EtOH$ and $[Zr(HL)_2Cl_4].H_2O.3EtOH$ have nearly similar behavior, indicating that they are iso-structurally and isothermally. TG curves show TG weight loss in the temperature range of 25-196°C due to removal of some solvents of crystallization. After that the TG curves register progressive weight losses 47.92 and 55.56% in the temperature ranges of 179-354 and 196-362°C for Hf(IV) and Zr(IV) complexes, respectively due to release of one mol of ligand and pyrolysis of the second one to eliminate $2N_2$ gas along with dechloronation and some of lattice solvents. The process associates with a sharp strong DTG peaks with T_{max}=254 and 262°C, respectively and accomplishes through a narrow temperature ranges signified that thermolysis started rapidly. This step followed by the final decomposition step for each Hf(IV) and Zr(IV) complexes which occurred within 354-700 and 362-700°C ranges and associated with a weak broad diffused DTG peaks 394, 453, 500 and 390, 432, 503°C, respectively. This step is characterized by weight losses 10.73 and 12.22% denoted to release of (5.75C +7H_2 gas) and (7C+2H_2 gas), respectively leaving oxygen molecule raised from rest solvent of crystallization to form MO_2 contaminated with carbon atoms as a final thermolysis product [54,55]. The thermal decomposition pathway of Hf(IV) complex is taken as representative example, Scheme 5.

Insert Scheme 5 and its caption here

The thermal decomposition of $[UO_2(HL)_3(NO_3)_2].3.75H_2O$ shows TG weight loss 2.95% in the temperature range of 23-169°C due to removal of 1.5 mol of hydrated water, however the rest of water removed with the decomposition of complex where it was involved in lattice [56]. The weight loss 7.15% within 169-202°C with DTG sharp peak at T_{max}=185°C corresponding to removal one mol of nitrate group plus 0.25 mol of water molecule. The second strong DTG peak in the temperature range of 202-291°C with T_{max}=285°C and associated with TG weight loss 21.26% attributed to elimination of one mol of ligand as well as two mol of lattice water molecules. The observed TG weight loss 9.22% estimated through a broad temperature range of 291-500°C equivalent to release of one mol of nitrate and two mol of methyl groups. After that the TG curve exhibits inflection at 500°C up to 741°C with 30.88% weight loss raised from

complete ligand pyrolysis leading to formation of UO_2 as a final product [57]. Scheme 6 describes the thermal decomposition processes of UO_2(II) complex.

Insert Scheme 6 and its caption here

The thermal analysis of all complexes carried out under nitrogen gas and the solvent of crystallization were responsible for the formation of metal oxides as final products from thermal decomposition [58].

Insert Table 3 and its caption here

3.6. XRD Analysis

X-ray powder diffraction analysis of Pd(II), Cr(III) and Zr(IV) metal complexes is carried out to determine the type of crystal system and lattice parameters. As shown in Figure S5. X-ray diffractograms of these metal complexes show good intense peaks indicating high crystallinity [59]. The results obtained from computational data reflected that Pd(II) complex had orthorhombic structure of P type lattice while Cr(III) and Zr(IV) complexes have monoclinic structure of P type lattice. Moreover, using the diffraction data, the mean crystallite sizes of the complexes (D) are determined according to the Scherrer equation ($D = 0.9\lambda/(\beta\cos\theta)$), where λ is X-ray wavelength, θ is Bragg diffraction angle, and β is the full width at half maximum of the diffraction peak [59]. The average crystallite sizes of complexes are found to be 83-113 nm. Cr(III) and Zr(IV) metal complexes are in nano-size. The values are given in Table 4.

Insert Table 4 and its caption here

3.7. Molecular modeling of (HL) ligand and its metal complexes

Molecular modeling is carried out to understand the “rules” that described chemical behavior of compounds and demonstrated the better geometrical structure for **HL** ligand [51]. Also, numbering of the ligand skeleton is observed and shown in Figure S6.

Spartan '14 V1.1.4 software is employed to carry out the quantum chemical calculations. Semi-Empirical (PM3) calculations are performed. Two different model structures are built for $[Fe(HL)_3Cl_2(OH)]$ and $[Pd(HL)_2Cl_2]$ complexes through nitrogen atom of NH_2 group (Figures S 7,9) or C=N (pyrazole) (Figures S 8,10). The data in Table 5 showed the total energy of the two proposed structures for Fe(III) and Pd(II) complexes in which, the ligand coordinates through NH_2 group are smaller than that the values where coordinated through C=N group. This is a better agreement with the experimental data (Figures S 7,9).

Insert Table 5 and their caption here

Quantum chemical parameters such as the highest occupied molecular orbital energy (E_{HOMO}), the lowest unoccupied molecular orbital energy (E_{LUMO}), energy gap (ΔE) and other parameters that give a valuable information about the reactive behavior, such as electronegativity (χ), chemical potential (μ), global hardness (η) and softness (σ) [60] are calculated quantitatively to depict the reactivity of the ligand and some complexes Table 6.

Absolute hardness (η) and softness (σ) are important properties to measure the molecular stability and reactivity. In a complex formation system, the ligand acts as a Lewis base while the metal ion acts as a Lewis acid. Metal ions are soft acids and thus soft base ligands are most effective for complex formation. A hard molecule has a large energy gap and a soft molecule has a small energy gap. Soft molecules are more reactive than hard ones because they could easily offer electrons. Ligand has higher softness (σ). It is more reactive and easily giving electrons to metal and possess high ability for complexation.

Global hardness and softness are important properties to measure the molecular stability and reactivity. The hardness values (Table 6) show that $[Fe(HL)_3Cl_2(OH)]$ and $[Pd(HL)_2Cl_2]$ are less harder than ligand, so the complexes have higher potential chemical resistance to change the number of electrons among the ligand. Also, $[Fe(HL)_3Cl_2(OH)]$ has higher value of global softness which indicated that the complex showed greater reactivity than its ligand. The energy gap (ΔE) is directly involved with hardness/softness of a chemical species. A lower value of ΔE made two complexes more reactive or low kinetic stability than their ligand. Computed the electrophilicity indexes were measured the stabilization energy when the system acquires an additional electronic charge from the environment. From the ω values (Table 6), the order of electrophilicity as following: $[Fe(HL)_3Cl_2(OH)]$ > Ligand > $[Pd(HL)_2Cl_2]$. $[Fe(HL)_3Cl_2(OH)]$ had the highest value of electrophilicity, which showed its high ability to accept electrons (the most reactive compound).

Insert Table 6 and its caption here

3.8. Biological Activity

3.8.1. Antitumor activity

The cytotoxic activity of the ligand and its Pd(II) and Ru(III) complexes is evaluated against breast MCF-7 cell line. The cytotoxicity of the tested compounds is expressed by (IC_{50}),

the biological screening results of tested compounds in *vitro* are listed in Table 7 and compared with the activity of doxorubicin as a reference drug.

Pd(II) complex shows high activity relative to free ligand and Ru(III) complex. Cytotoxic activity of the complexes may be attributed to the central metal atom as explained by Tweedy's chelation theory [51]. The cytotoxic activity of complexes resulted from the binding of metal ions with DNA and forming cross links, these binding caused distortion of the helical structure of DNA and by this DNA replication inhibited. It seems that the nature of the metal ion had an effect on the biological behaviour. The Pd(II) complex shows high activity rather than other tested compounds under the same experimental conditions. On screening, it is observed that Pd-3-amino-4,6-dimethyl-1*H*-pyrazolo[3,4-b]pyridine is more toxic than Ru-3-amino-4,6-dimethyl-1*H*-pyrazolo[3,4-b]pyridine against the studied cell line. This occurred because of the slow ligand-exchange of Ru(III) compounds, due to the high tendency of Ru(III) ion to form strong bonds with ligand and it can bind with other biomolecules in the cell rather than DNA. Also, the square planar geometry around Pd(II) ion, made Pd(II) ion more flexible for reaching to DNA rather than the restricted octahedral Ru(III) ion [61-63].

Insert Table 7 and its caption here

3.8.2. Antimicrobial Activity

Using the paper disk diffusion method, the ligand and some of its metal complexes are evaluated for their antimicrobial activities. Thus, these compounds are screened against *Staphylococcus aureus*; *Bacillus cereus* as a Gram-positive bacteria and *Escherichia coli*; Pseudomonas aeruginosa as Gram-negative bacteria (Table 8). The ligand and its tested complexes have weak activity towards a Gram-positive bacteria and no activity towards Gram-negative bacteria except Pd(II) complex has observed activity towards *Pseudomonas aeruginosa*.

Insert Table 8 and its caption here

Conclusion

Mn(II), Pd(II), Fe(III), Cr(III), Ru(III), Hf(IV), Zr(IV) and UO_2(II) metal complexes of 3-amino-4,6-dimethyl-1*H*-pyrazolo[3,4-b]pyridine ligand are prepared. Spectral (IR, UV–visible, ^{1}H NMR and mass spectra), magnetic and thermal studies confirm the structure of the ligand and its metal complexes. IR spectra show that the ligand coordinates to all metal ions as a neutral monodentate moiety through nitrogen atom of amino group. The ligand to metal (L:M) stoichiometry is found to be 2:1 and 3:1. The electronic absorption spectra along with magnetic

measurements suggest octahedral geometry for all synthesized metal complexes, except Pd(II) complex. The X- ray diffraction studies suggest orthorhombic structure of P type lattice for Pd(II) complex and monoclinic structure of P type lattice for Cr(III) and Zr(IV). Theoretical calculations are performed to support the experimental results. Pd(II) complex presents a higher antitumor activity against MCF-7 cell line. The synthesized ligand and its Pd(II), Cr(III) and Zr(IV) metal complexes also are screened for antibacterial activity.

Acknowledgment

We would like to acknowledge the financial support of the Menoufia University

References

[1] M.A. Gouda, Utility of 3-Amino-4,6-dimethyl-1H-pyrazolo[3,4-b]pyridine in Heterocyclic SynthesiJ. Heterocycl. Chem. 48 (2011) 1-10.

[2] L.F. Pedrosa, W.P. de Macedo, A.C.R. Furtado, G.P. Guedes, J.C. Borges, J.A.L.C. Resende, M.G.F. Vaz, A.M.R. Bernardinoa, M.C. de Souza, Synthesis and characterization of new 1*H*-pyrazolo[3,4-*b*]pyridine phosphoramidate derivatives, ARKIVOC iv (2014) 38-50.

[3] V. Kumar, V. Sareen, V. Khatri, S. Sareen, Recent applications of pyrazole and its substituted Analogs, IJAR 2016; 2(9): 461-469.

[4] T. Tuccinardi, A.T. Zizzari, Ch. Brullo, S. Daniele, F. Musumeci, S. Schenone, M.L. Trincavelli, C. Martini, A. Martinelli, G. Giorgi, M. Botta, Substituted pyrazolo[3,4-b]pyridines as human A(1) adenosine antagonists: Developments in understanding the receptor stereoselectivity, Org. Biomol. Chem. 9 (2011) 4448-4455.

[5] M.A.M. GAD-ELKAREEM, A.M. ABDEL-FATTAH, A.A. ELNEAIRY Y, Pyrazolo[3,4-b]pyridine in heterocyclic synthesis: synthesis of new pyrazolo[3,4-b]pyridines, imidazo[1',2':1,5]pyrazolo[3,4-b]pyridines and pyrido[2',3':3,4]pyrazolo[1,5-a]pyrimidines, CAN. J. CHEM. 85 (2007) 592–599.

[6] H.H. Ibraheem, Kh.F. Suhail, Sh.S. Hasan, Synthesis and Characterization of Hetrocyclic Compounds Derived from ethyl-4-aminobenzoateAl-Nahrain Univ. J. 21 (2018) 57-63.

[7] Y.K. Abdel-Monem, S.A. Abou El-Enein, M.M. El-Sheikh-Amer, Design of new metal complexes of 2-(3-amino-4,6-dimethyl-1H-pyrazolo[3,4-b]pyridin-1-yl)aceto-

hydrazide: Synthesis, characterization, modelling and antioxidant activity J. Mol. Stru 1127 (2017) 386-396.

[8] Y.K. Abdel-Monem, S.M. Emam, H.M. Okda. Solid state thermal decomposition synthesis of CuO nanoparticlesfrom coordinated pyrazolopyridine as novel precursors, J. Mater. Sci. Mater Electron. 28 (2017) 2923-2934.

[9] H.E. Gaffer, T.K. A. Khattab, Synthesis and Characterization of Some Azo-heterocycles Incorporating pyrazolopyridine Moiety as Disperse Dyes, Egypt J. chem 60 (2017) 41-47.

[10] O.O. James, K.O. Ajanaku, K.O. Ogunniram, O.O. Ajani, T.O. Sinabola, M.O. John, Adsorption Behaviour of Pyrazolo [3, 4-b] Pyridine on Corrosion of Stainless Steel in HCl Solutions, Trends, Appl. Sci. Res. 69 (2011) 910-917.

[11] M.P. Campello, E. Palma, I. Correia, P.M.R. Paulo, A. Matos, J. Rino, J. Coimbra, J.C. Pessoa, D. Gambino, A. Paulo, F. Marques, Lanthanide complexes with phenanthroline-based ligands: insights into cell death mechanisms obtained by microscopy techniques
Dalton Trans. 48 (2019) 4611-4624.

[12] S. Verma, S. Shrivastva, R. Shrivastva, Synthesis, Characterization, and Physicochemical studies of mixed ligand complexes of inner transition metals with lansoprazole and cytosine, J. Chem. 2013, http://dx.doi.org/10.1155/2013/309179.

[13] J. Bassett, R.C. Denney, G.H. Jeffery, J. Mendham, Vogel's Textbook of Quantitative Inorganic Analysis Including Elementary Instrumental Analysis, 4th ed., Longman Group, London, 1978.

[14] J. Lewis, R.G. Wilkins, Modern Coordination Chemistry, Interscience, New York, 1960, 403.

[15] F.A. Yassin, Synthesis, reactions and biological activity of 2-substituted 3-cyano-4,6-dimethylpyridine derivatives, Chem. Heterocycl. Compd. 45 (2009) 35-41.

[16] A. Lawson, R.B. Tnkler, Chemistry of thiadiazole and thiadiazine S-oxides, Chem. Rev. 70 (1970) 593-618.

[17] T. Mosmann, Rapid colorimetric assay for cellular growth and survival: application to proliferation and cytotoxicity assays, J. Immunol. Methods 65 (1983) 55-63.

[18] A.P. Singh, N.K. Kaushik, A. Verma, G. Hundal, R. Gupta, Synthesis, structure and biological activity of copper(II) complexes of 4-(2-pyridylmethyl)-1,7-dimethyl-1,4,7-triazonane-2,6-dione and 4-(2-pyridylethyl)-1,7-dimethyl-1,4,7-triazonane-2,6-dioneEur. J. Med. Chem. 44 (2009) 1607-1614.

[19] F.V. Nussbaum, B. Miller, S. Wild, C.S. Hilger, S. Schumann, H. Zorbas, W. Beck, W. Steglich, Synthesis of 1-(2-Aminophenyl)isoquinolines and the Biological Activity of Their cis-Dichloro Platinum(II) Complexes, J. Med. Chem. 42 (1999) 3478-3485.

[20] National Committee for Clinical Laboratory Standards. Methods for determining bactericidal activity of antimicrobial agents. Tentative guidelines. National Committeefor Clinical Laboratory Standards document M26-T (vol. 12, no. 19).Villanova, PA: NCCLS; 1992.

[21] Clinical and Laboratory Standards Institute (CLSI) (2017). Performance Standards for Antimicrobial Susceptibility Testing. M100, 27th ed. January 2017 Replaces M100-S26

[22] C. Anitha, C.D. Sheela, P. Tharmaraj, S. Sumathi, Spectroscopic studies and biological evaluation of some transition metal complexes of azo Schiff-base ligand derived from (1-phenyl-2,3-dimethyl-4-aminopyrazol-5-one) and 5-((4-chlorophenyl)diazenyl)-2-hydroxybenzaldehyde, Spectrochim. Acta A 96 (2012) 493-500.

[23] A.M. Khedr, F.A. Saad, Synthesis, structural characterization, and antimicrobial effciency of sulfadiazine azo-azomethine dyes and their bi-homonuclear uranyl complexes for chemotherapeutic use, Turk. J. Chem. 39 (2015) 267-280.

[24] H.H. Monfared, R. Bikas, J. Sanchiz, T. Lis, M. Siczek, J. Tucek, R. Zboril, P. Mayer, Syntheses, structures and magnetic properties of azido- and phenoxo-bridged complexes of manganese containing tridentate aroylhydrazone based ligands, Polyhedron 61 (2013) 45-55.

[25] M.M. Abd-Elzaher, M.M. E. Shakdofa, H.A. Mousa, S.A. Moustafa, Synthesis, characterization and biological activity of some ferrocenyl complexes containing antipyrine moiety, Sop Trans. Appl. Chem. 1 (2014) 42-52.

[26] N.N. Pesyan, D. Soleimani, N.H. Jazani, New tetrazolic azo dyes linked to (thio)barbiturate and electron-rich aromatics as potential antimicrobial agents, Turk J Chem. 39 (2015) 998-1011.

[27] R. Fikry, N. Ismail, S. Raslan, H. El-Tahawe, Synthesis and reactions of new pyrazole derivatives, Eur. Chem. Bull. 5 (2016) 157-162.

[28] Z. Seferoğlu, A study on tautomeric equilibria of new hetarylazo-6-aminouracils, ARKIVOC. vii (2009) 42-57.

[29] M.S. Masoud, S.A.A. El-Enein, H.M. Kamel, Structural chemistry and thermal properties of some pyrimidine complexes, Indian. J. Chem. A 41 (2002) 297-303.

[30] S. Deepak, A. Rakshit, V. Ritu, Microwave-assisted synthesis of some biologically active pyrazole derivatives, J. Pharm. Sci. Innov. 3 (2014) 463-467.

[31] M.S. Masoud, S.A.A. El-Enein, M.E. Ayad, A.S. Goher, Spectral and magnetic properties of phenylazo-6-aminouracil complexes, Spectrochim.Acta A 60 (2004) 70-87.

[32] Y.K. Abdelmonem, F.A. EL-Essawy, S.A. Abou El-Enein, M.M. El-Sheikh-Amer, Docking Studies, Synthesis, and Evaluation of Antioxidant Activities of N-Alkylated, 1,2,4-Triazole, 1,3,4-Oxa-, and Thiadiazole Containing the Aminopyrazolopyridine Derivatives, Int. J. Org. Chem. 3 (2013) 198-205.

[33] P. Tyagi, S. Chandra, B.S. Saraswat, Ni(II) and Zn(II) complexes of 2-((thiophen-2-ylmethylene)amino)benzamide: synthesis, spectroscopic characterization, thermal, DFT and anticancer activities, Spectrochim. Acta A 134 (2015) 200-209.

[34] M.S. Masoud, A. El-Marghany, A. Orabi, A.E. Ali, R. Sayed, Spectral, coordination and thermal properties of 5-arylidene thiobarbituric acids, Spectrochim. Acta A 107 (2013) 179-187.

[35] E. Canpolat, Synthesis and Characterization of Dioxouranium (VI) Complexes of Schiff Bases (Mixed-Ligads Part 1), BEU J. Sci. 3 (2014) 74-80.

[36] H.A. El-Boraey, S.M. Emam, D.A. Tolan, A.M. El-Nahas, Structural studies and anticancer activity of a novel (N6O4) macrocyclic ligand and its Cu(II) complexes, Spectrochem. Acta. A 78 (2011) 360-370.

[37] P.E. Hansen, J. Spanget-Larsen, NMR and IR investigations of strong intramolecular

hydrogen bonds, Molecules 22 (2017) 562-573.

[38] B. Kebede, N. Retta, J.V.T. Raju, Y. Chebude, Synthesis and Characterization of 2, 4, 6-tris (hydrazino)-s-triazine and its Metal Complexes, Trans. Met. Chem. 31 (2006) 19-26.

[39] S.M. Emam, I.E. El Sayed, N. Nassar, Transition metal complexes of neocryptolepine analogues. Part I: synthesis, spectroscopic characterization, and invitro anticancer activity of copper(II) complexes, Spectrochim. Acta A 138 (2015) 942-953.

[40] A.B.P. Lever, Inorganic electronic spectroscopy, 2nd edn. Elsevier, Amsterdam 1984.

[41] M. Gaye, F.B. Tamboura, A.S. Sall, Spectroscopic studies of some lanthanide(III) nitrate complexes synthesized from a new ligand 2,6-bis-(salicylaldehyde hydrazone)-4-chlorophenol, Bull. Chem. Soc. Ethiop. 17 (2003) 27-34.

[42] S.K. Patil, V.M. Naik, D.C. Bilehal, N.B. Mallur, Synthesis, Spectral and Antimicrobial Studies of Lanthanide (III) Nitrate Complexes with Terdentate ONO Donor Hydrazones, J. Exp. Sci. 2 (2011) 15-20.

[43] S.M. Emam, S.A.A. El-Enein, F.A. El-Saied, S.Y. Alshater, Synthesis and characterization of some bi, tri and tetravalent transition metal complexes of N'-(furan-2-yl-methylene)-2-(p-tolylamino)acetohydrazide HL^1 and N'-(thiophen-2-yl-methylene)-2-(p-tolylamino)acetohydrazide HL^2.Spectrochim. Acta A 92 (2012) 96-104.

[44] S.A.A. El-Enein, S.M. Emam, M.W. Polis, E.M. Emara, Synthesis and characterization of some metal complexes derived from azo compound of 4,4′-methylenedianiline and antipyrine: Evaluation of their biological activity on some land snail species, J. Mol. Struct. 1099 (2015) 567-578.

[45] R. Shukla, P.K. Bharadwaj, Synthesis and characterization of a mononuclear iron(III) complex with a tripodal triamide ligand, Polyhedron 12 (1993) 1553-1557.

[46] P.B. Tsitovich, F. Gendron, A.Y. Nazarenko, B.N. Livesay, A.P. Lopez, M.P. Shores, J. Autschbach, J.R. Morrow, Low-spin Fe(III) macrocyclic complexes of imidazole-appended1,4,7-triazacyclononane as paramagnetic probes, Inorg. Chem. XXXX, DOI:

10.1021/acs.inorgchem.8b01022.

[47] P.U. Gawande, P.R. Mandlik, A.S. Aswar, Synthesis and characterization of Cr(III), Mn (III), Fe(III), VO(IV), Zr(IV) and UO_2(VI) complexes of Schif base derived from isonicotinoyl hydrazine, Indian J Pharm Sci. 77 (2015) 376–381.

[48] N. Raja, R. Ramesh, Mononuclear ruthenium(III) complexes containing chelating thiosemicarbazones: Synthesis, characterization and catalytic property, Spectrochim. Acta A 75 (2010) 713-718.

[49] Y.K. Abdelmonem, S.A.A. El-Enein, S.M. El-Seady, Synthesis, characterization and molecular modeling of some transition metal complexes of Schiff base derived from 5-aminouracil and 2-benzoyl pyridine, J. Mol. Struct. 1152 (2018) 115-127.

[50] G.J. Kharadia, J.R. Patel, B. Z. Dholakiya, Antituberculosis, antifungal and thermal activity of mixed ligand transition metal complexes, Appl. Organometal. Chem. 24 (2010) 821–827.

[51] S.A.A. El-Enein, S.M. Emam, F.I. Abouzayed, Synthesis, spectral characterization, thermal studies and biological activity of (Z)-5-((1,5-dimethyl-3-oxo-2-phenyl-2,3-dihydro-1H-pyrazol-4-yl)diazenyl)-6-hydroxy-2-mercaptopyrimidin-4(3H)-one and its metal complexes, Appl. Organometal. chem. (2017) DOI: 10.1002/aoc.4073.

[52] M.S. Masoud, A.E. Ali, M.A. Shaker, G.S. Elasala, Synthesis, computational, spectroscopic, thermal and antimicrobial activity studies on some metal-urate complexes, Spectrochim. Acta A 90 (2012) 93-108.

[53] H.A. El-Boraey, O.A. EL-Gammal, Novel (N4) Macrocyclic Metal Complexes: Synthesis, Characterization, Spectral Studies and Anticancer Activity, Open Chem. J. 6 (2019) 51-63.

[54] A.S. El-Tabl, F.A. El-Saied, A.N. Al-Hakimi, Synthesis, spectroscopic investigation and biological activity of metal complexes with ONO trifunctionalalized hydrazone ligand, Transition Met. Chem. 32 (2007) 689-701.

[55] S.A. Sadeek, W.H. El-Shwiniy, W.A. Zordok, E. Kotb, Spectroscopic studies, thermal analyses and biological evaluation of new V(IV), Zr(IV) and U(VI) moxifloxacin complexes, J. Mol. Struct. 1006 (2011) 192-209.

[56] M.S. Masoud, S.A.A. El-Enein, A.M. Ramadan, A.S. Goher, Thermal properties of some biologically active 5-(p-substituted phenylazo)-6-aminouracil complexes, J. Anal. Appl. Pyrolysis. 81 (2008) 45-51.

[57] H.A. El-Boraey, F.A. El-Saied, S.A. Aly, UO_2(VI), Sn(IV), Th(IV) and Li(I) complexes of 4-azomalononitrile antipyrine, J. Therm. Anal. Calorim. 96 (2009) 599-606.

[58] S.M. Emam, S.A. Abou El-Enein, E.M. Emara, Spectroscopic studies and thermal decomposition for (bis-((E)-2-(4-ethylphenylimino)-1,2-diphenylethanone) Schiff base and its Co(II), Ni(II), Cu(II), Zn(II) and Cd(II) complexes prepared by direct and template reactions, J. Therm. Anal. Calorim. 127 (2017) 1611-1630.

[59] M. Bal, G. Ceyhan, B. Avar, M. Kose, A. Kayraldiz, M. Kurtoglu, Synthesis and X-ray powder diffraction, electrochemical, and genotoxic properties of a new azo-Schiff base and its metal complexes, Turk J Chem 38 (2014) 222-241.

[60] C. Verma, M.A. Quraishi, E.E. Ebenso, Adsorption and Inhibition Behavior of Purine based Drugs on Mild Steel Corrosion in Hydrochloric Acid Solution: DFT Study, Anal. Bioanal. Electrochem. 10 (2018) 98-110.

[61] N.T.A. Ghani, A.M. Mansour, Novel Pd(II) and Pt(II) complexes of N,N-donor benzimidazole ligand: Synthesis, spectral, electrochemical, DFT studies and evaluation of biological activity, Inorg. Chim. Acta, 373 (2011) 249-258.

[62] M.B. Baile, N.S. Kolhe, P.P. Deotarse, A.S. Jain, A.A. Kulkarni, Metal Ion Complex - Potential Anticancer Drug-A Review, Inter. J. Pharm. Res. Rev. 4 (2015) 59-66.

[63] S.A.A. El-Enein, S.M. Emam, E. Monir, Spectrochemical and Thermal Studies for Bivalent Metal Complexes of Azodye Ligand Containing Pyrimidine RingInter. J. Eng. Res. Tech. (IJERT) 6 (2017) 353-364.

No.		F.W. (g/mol) Color	Elemental analyses Found/(Calcd.)% C	H	N	Cl	M	Λ^*
	HL $C_8H_{10}N_4$	162.26 Buff	59.31 (59.24)	6.19 (6.21)	33.95 (34.34)	- -	- -	- -
1	$[Mn(HL)_3Cl_2(H_2O)].1.5H_2O$ $C_{24}H_{33}N_{12}O_{2.5}MnCl_2$	657.54 Light brown	43.80 (43.84)	5.28 (5.37)	25.69 (25.56)	10.63 (10.80)	8.20 (8.36)	8
2	$[Pd(HL)_2Cl_2].H_2O.2EtOH$ $C_{20}H_{34}N_8O_3PdCl_2$	611.87 Yellowish brown	39.19 (39.26)	5.48 (5.61)	21.19 (18.31)	11.59 (11.23)	17.39 (17.22)	13
3	$[Fe(HL)_3Cl_2(OH)].4.5H_2O.3.75EtOH$ $C_{31.5}H_{63.5}N_{12}O_{9.25}FeCl_2$	885.43 Dark brown	42.94 (42.78)	7.11 (7.17)	20.12 (19.54)	7.70 (8.16)	6.83 (6.31)	16
4	$[Cr(HL)_3Cl_3].3EtOH$ $C_{30}H_{48}N_{12}O_3CrCl_3$	783.15 Deep buff	46.41 (46.02)	6.54 (6.17)	22.12 (21.56)	14.80 (13.58)	7.10 (6.63)	11
5	$[Ru(HL)_3Cl_3].9.5EtOH$ $C_{43}H_{87}N_{12}O_{9.5}RuCl_3$	1131.87 Black	45.56 (45.59)	7.92 (7.69)	14.74 (14.84)	9.52 (9.41)	11.21 (11.11)	17
6	$[Hf(HL)_2Cl_4].4H_2O.1.5EtOH$ $C_{19}H_{37}N_8O_{5.5}HfCl_4$	786.36 Deep yellow	28.80 (29.04)	5.12 (4.75)	16.54 (14.40)	18.27 (18.05)	22.90 (22.72)	24
7	$[Zr(HL)_2Cl_4].H_2O.3EtOH$ $C_{22}H_{40}N_8O_4ZrCl_4$	713.65 Yellowish green	37.38 (37.02)	5.37 (5.64)	16.20 (15.70)	18.97 (19.87)	12.12 (11.78)	17
8	$[UO_2(HL)_3(NO_3)_2].3.75H_2O$ $C_{24}H_{37.5}N_{14}O_{11.75}U$	949.05 Yellow	39.71 (39.83)	4.41 (4.00)	21.34 (20.75)	- -	25.57 (25.08)	5

Table 1
Analytical and Physical Data of **HL** Ligand and Its Metal Complexes

No.	Compound	υ NH_2 (asym) + υ NH_2 (sym)	υ(NH)	δ(NH_2), υ(C=N)	δ(NH)	ν(C-NH_2), ν(N-N)	Pyrazol ring breathing+ roking(NH_2), Py ring	γ(NH)	Pyring bending,in plane	Py ring bending out-of- plane	ρ NH_2	ν(M-N)
	HL	3397s 3290m	3190m 3114sh	1623, 1607sp	1459m 1407s	1312m 1127w	1074s 1023m	772w 656w	615s 579w	435w	491m	-
1	$[Mn(HL)_3Cl_2(H_2O)].1.5\ H_2O$	3396w 3275w	3191w 3101w	1637s, 1603s	1455s 1419m	1308m 1122w	1054s 1024sh	779s 653m	621m 587m	442sh	500w	544w
2	$[Pd(HL)_2Cl_2].H_2O.2EtOH$	3433w 3304b.m	3202w 3102vw	1637m, 1607w	1445m 1415w	1303sh 1120w	1084m 1033m	775m 643m	608sh 582m	442w	498w	542w
3	$[Fe(HL)_3Cl_2OH].4.5.H_2O.$ 3.75 EtOH	3378sh 3324b.s	3202m 3159w	1647s, 1614w	1445m 1386m	1298sh 1127m	1082w 1035m	770m 654w	615m 576w	441w	480m	546w
4	$[Cr(HL)_3Cl_3].3EtOH$	3397s 3296s	3193m 3104m	- 1606s	1454s 1412s	1315m 1122w	1068m 1027m	769s 653m	616m 581w	438w	494w	547w
5	$[Ru(HL)_3Cl_3].9.5EtOH$	3409b.s 3294b.s	- 2986w	- 1598s	1444s 1398	1300w 1121w	1079m 1038s	775sh 624m	624m 581vw	424w	488w	536w
6	$[Hf(HL)_2Cl_4].4H_2O\ 1.5EtOH$	3383w 3324s	3202s 3083sh	1652s, 1609m	1437m 1400	1293w 1132w	1093s 1041m	773m 650m	615m 578w	436sh	477m	539w
7	$[Zr(HL)_2Cl_4].H_2O\ 3EtOH.$	3417m 3327s	3201s 3153w	1642s, 1604w	1444s 1383m	1302sh 1123w	1076v.w 1036m	764m 651w	604m 581sh	436sh	475w	537w
8	$[UO_2(HL)_3(NO_3)_2].3.75.H_2O$	3398s 3322s	3206s 3093w	1647s, 1605m	1434s 1387s	1295m 1134w	1071vw 1036m	773m 663w	610m 573w	443sh	481w	526w

s: strong, m:medium, w:weak, b:broad, b.m: broad medium, v.w: very weak, sh: shoulder, and b.s: broad strong

Table 2.

Infrared Bands (cm^{-1}) and Their Assignments for ligand (HL)and Its Metal Complexes

No.	Compound	TG range (°C)	DTG peak (°C)	Mass Loss % Found	Mass Loss % Calcd.	Assignment	T_S (°C)
	HL.	25-164	-	-	-	Stable	164
		164-400	282	98.29	98.53	Ligand pyrolysis [d]	
		At 400	-	1.63	1.45	0.25C [r]	
1	$[Mn(HL)_3\ Cl_2(H_2O)].1.5H_2O$	25-181	34-67	2.42	2.32	loss of one mol H_2O [a]	181
		181-266	248	28.07	27.63	loss of (one mol of P.Py+0.5 mol of Cl_2) [b,d]	
		266-345	302	33.35	33.11	loss of (one mol of P.Py+0.5 mol of Cl_2+3mol of C)	
		345-542	377,428,498	19.97	19.77	loss of (3 mol of N_2 gas+8 mol of H_2 gas+2.5 mol of C)	
		At 542	-	16.53	16.58	0.5 Mn_2O_3 +2.5C [r]	
2	$[Pd(HL)_2Cl_2].H_2O.2EtOH$	25-202	45,148	8.42	8.58	loss of (one mol H_2O +0.75 mol of EtOH) [a,b]	202
		202-354	303	29.06	29.70	loss of (one mol of P.Py+0.5 mol of Cl_2) [d]	
		354-727	392, 456	42.08	41.71	loss of (one mol of NH_2+2.75 mol of H_2 +0.25 mol of H_2O+2.5 mol of C+0.5 mol of Cl_2+ ligand pyrolysis) [d]	
		At 727	-	20.48	20.00	PdO [r]	
3	$[Fe(HL)Cl_2\ OH)].4.5.H_2O.3.75EtOH$	25-127	102	6.59	6.44	loss of 1.25 mol of EtOH [a]	237
		127-237	186	20.60	20.90	loss of (4 mol of H_2O+2.5 mol of EtOH)	
		237-419	300,332	12.25	12.30	loss of (one mol of Cl_2+2 mol of (CH_3+H_2)) [d]	
		419-651	480, 577	48.25	48.69	loss of (2 mol of L+ ligand pyrolysis)	
		At 651	-	12.09	12.15	0.5Fe_2O_3 [r]	
4	$[Cr(HL)_3Cl_3].3EtOH$	25-194	43	8.47	8.81	loss of 1.5 mol of EtOH [b]	194
		194-308	243	25.40	25.47	loss of (one mol of p.py+0.5mol of Cl_2+1.5mol of C) [b,d]	
		308-604	380, 508	48.74	48.27	loss of (2mol of ligand +one mol of NH_2+one mol of Cl_2+1.5 mol of C+4.5mol of H_2)	
		At 604	-	17.39	17.37	0.5Cr_2O_3 +5C [r]	
5	$[Ru(HL)_3Cl_3].9.5EtOH$	25-146	45	9.11	9.05	loss of 2.25 mol of EtOH [b]	146
		146-378	190,239,318	35.54	35.42	loss of (4 mol of EtOH+one mol of P.Py+one mol of Cl_2) [b,d]	
		378-644	427,542,614	44.61	44.64	loss of (0.5 mol of Cl_2+3 mol of C+1.75mol of H_2O+4.5 mol of H_2+2 mol of ligand+one mol of NH_2) [b,d]	
		At 644	-	11.21	11.11	0.5Ru_2O_3 [r]	
6	$[Hf(HL)_2Cl_4].4H_2O.1.5EtOH$	25-179	46,115	`10.8	11.07	loss of (1.5 mol of EtOH+ one mol of H_2O] [b,a]	179
		179-354	254	47.92	48.10	loss of (one mol of H_2O+2mol of Cl_2+2mol of N_2+one mol of ligand) [d]	
		354-700	394,453, 500	10.73	10.65		
		At 700	-	30.54	30.22	loss of (5.75mol of C+ 7mol of H_2) [d] HfO_2+2.25C [r]	

[a] :Dehydration, [b] :Desolvation, [d] :Decomposition and [r] :final residue

Table 3. TGA Analysis of **HL** Ligand and Its Metal Complexes

No.	Compound	TG range (°C)	DTG peak (°C)	Mass Loss % Found	Mass Loss % Calcd.	Assignment	T_S (°C)
7	$[Zr(HL)_2Cl_4].H_2O.3EtOH$	25-196	49	9.53	9.67	Loss of 1.5 mol of EtOH [b]	196
		196-362	262	55.56	55.62	Loss of (0.5 mol of EtOH+ 2 mol of Cl_2 +one mol of ligand +2 mol of N_2 +7 mol of H_2) [b,d]	
		362-700	390, 32,503	12.22	12.33	Loss of (7mol of C+2 mol of H_2) [d]	
		At 700	-	22.69	22.31	ZrO_2+3C [r]	
8	$[UO_2(HL)_3(NO_3)_2].3.75.H_2O$	23-169	56	2.95	2.06	Loss of 1.5 mol of H_2O [a]	201
		169-202	185	7.15	7.91	Loss of (one mol of NO_3+0.25 mol of H_2O) [b]	
		202-291	285	21.26	20.9	Loss of (one mol of ligand +2 mol of H_2O) [d]	
		291-500	-	9.22	9.71	loss of (one mol of NO_3+2mol of CH_3) [d]	
		500-741	614	30.88	31.01	complete ligand pyrolysis [d]	
		At 741	-	28.5	28.47	UO_2 [r]	

[a] :Dehydration, [b] :Desolvation, [d] :Decomposition and [r] :final residue

Table 3. *Continued*

Complex	a (Å)	b (Å)	c (Å)	D	Crystal structure
$[Pd(HL)_2Cl_2].H_2O.2EtOH$	9.578	16.376	17.439	113	Orthorhombic
$[Cr(HL)_3Cl_3].3EtOH$	6.552	16.436	13.141	83	Monoclinic
$[Zr(HL)_2Cl_4].H_2O.3EtOH$	8.767	4.893	25.862	97	Monoclinic

Table 4.
XRD Parameters of Pd(II), Cr(III) and Zr(IV) Complexes

Parameter	Fe(III)-NH_2	Fe(III)-C=N	Pd (II)-NH_2	Pd (II)-C=N
E_{HOMO} (eV)	-5.15	-6.62	-5.84	-7.86
E_{LUMO} (eV)	-2.31	-1.05	-0.61	-1.33
ΔE (eV)	2.84	5.57	5.23	6.53
Dipole Moment (debye)	14.02	7.14	2.13	10.51
Energy ($KJ.mol^{-1}$)	638.95	858.88	696.95	890.9

Table 5.

Energy gap ΔE (eV), Dipole Moment (debye) and Total Energy ($KJ.mol^{-1}$) of The Two Proposed Structure Computed at Ground State Level by PM3 Calculation

Compound	E_{HOMO}	E_{LUMO}	ΔE	χ	μ	η	σ	ω
ligand	-7.97	-0.33	7.64	4.15	-4.15	3.82	0.26	2.25
$[Fe(HL)_3(OH)Cl_2]$	-5.15	-2.31	2.84	3.73	-3.73	1.42	0.70	4.90
$[Pd(HL)_2Cl_2]$	-5.84	-0.61	5.23	3.23	-3.23	2.16	0.38	1.98

Table 6.

Quantum Chemical Parameters of Compounds Calculated by PM3 Method

Compound	IC_{50} (Mg/mL)
Doxorubicin	39.18
HL	55.15
$[Pd(HL)_2Cl_2]$	34.85
$[Ru(HL)_3Cl_3].9.5EtOH$	54.33

Table 7.

Cytotoxic Activity of **HL** Ligand and its Pd(II) and Ru(III) Complexes on Breast MCF-7 Cell Line

Compound	Bacterial strain			
	Gram (+)		Gram (-)	
	S. Aureus	*B. Cereus*	*E. Coli*	*P. Aeruginosa*
HL	12	8	-	-
$[Pd(HL)_2Cl_2]$	16	13	-	13
$[Cr(HL)_3Cl_3].3EtOH$	10	6	-	-
$[Zr(HL)_2Cl_4].H_2O.3EtOH$	11	7	-	-
SXT	25	36	27	19
control	7	5	-	-

Table 8.

Antibacterial Activity of **HL** Ligand and Some of its Metal Complexes

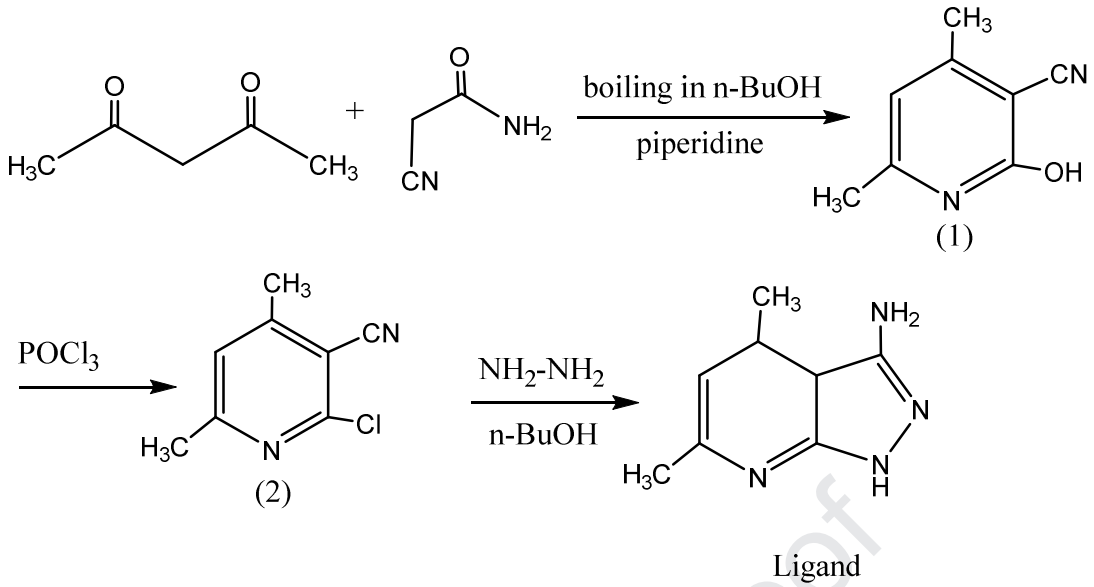

Scheme 1. Preparation of 3-Amino-4,6-dimethyl-1*H*-pyrazolo[3,4-b]pyridine (**HL**) ligand

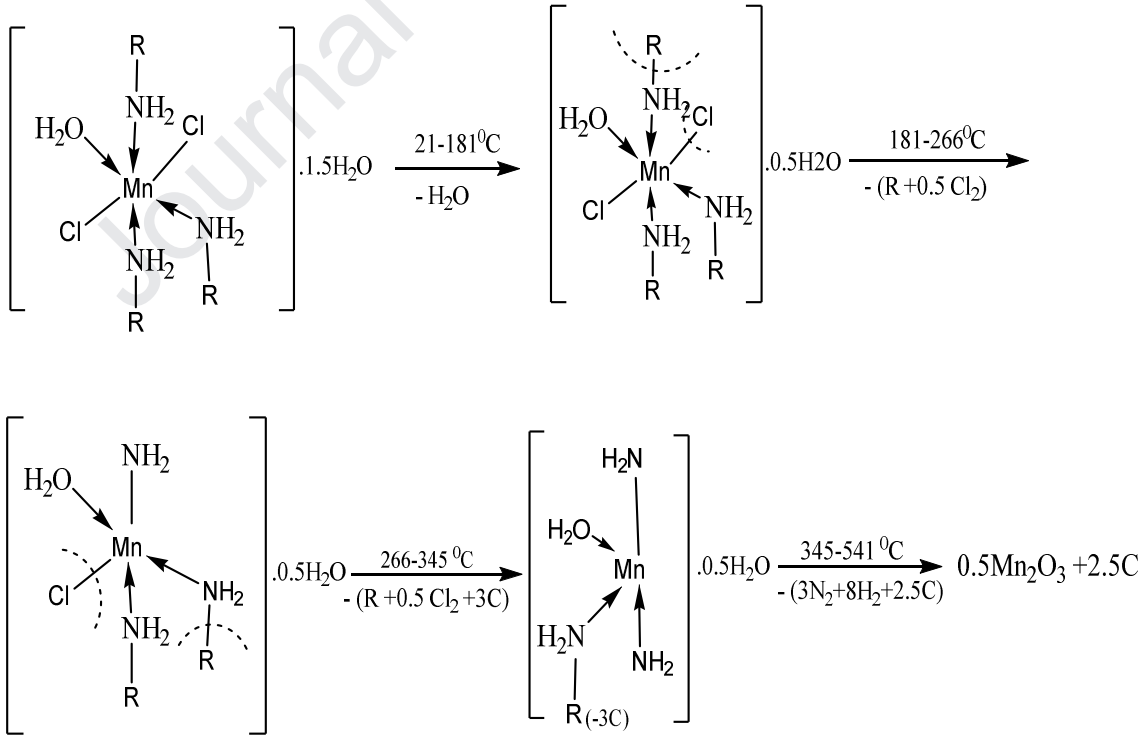

Scheme 2. The thermal decomposition pathway of Mn(II) complex

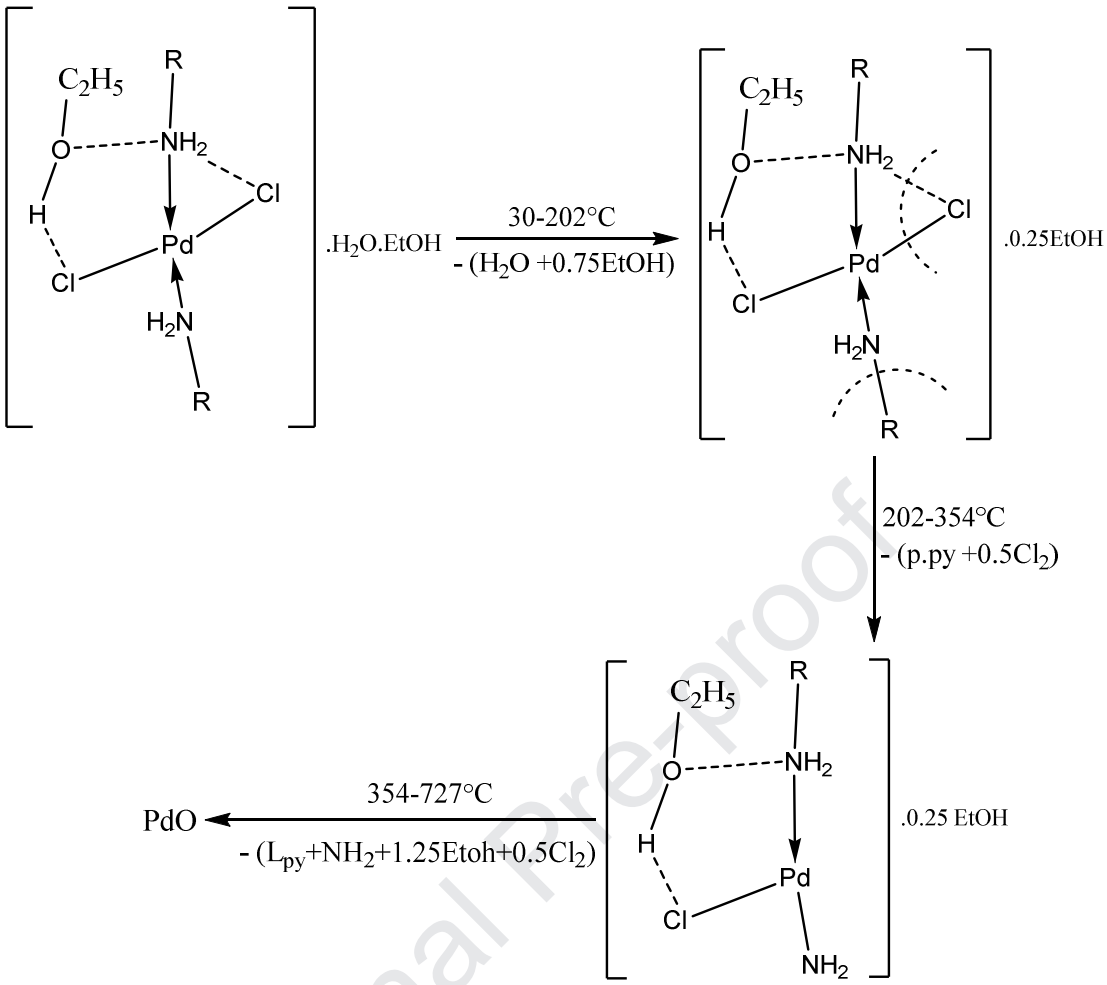

Scheme 3. Thermal decomposition of Pd(II) complex

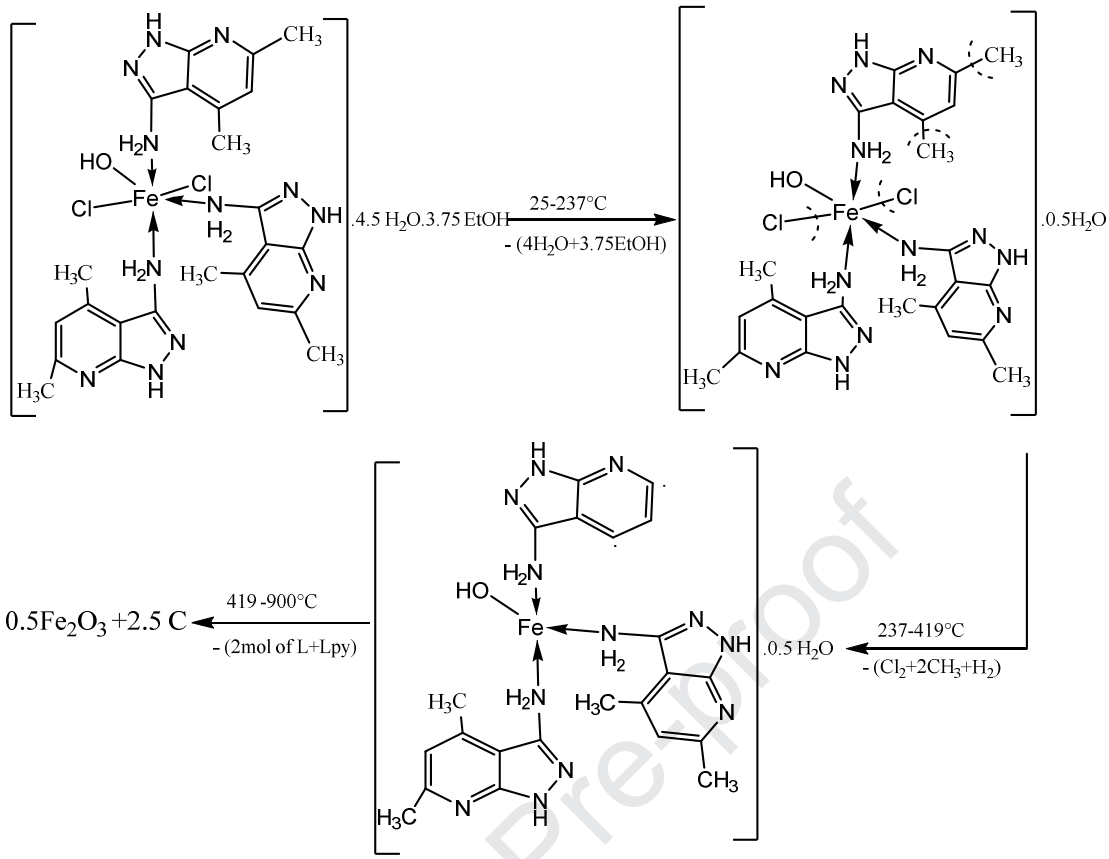

Scheme 4. Thermal decomposition of Fe(III) complex

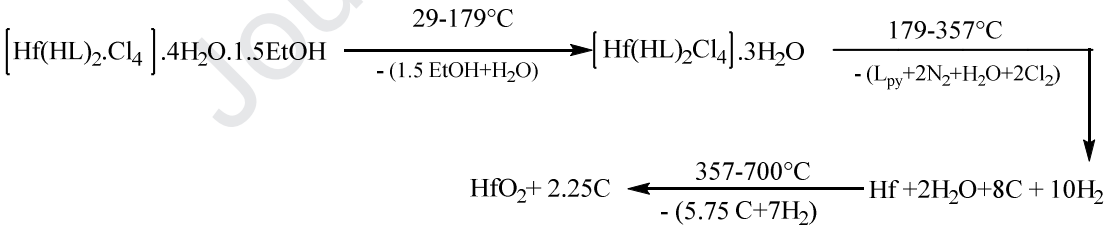

Scheme 5. Thermal decomposition pathway of Hf(IV)

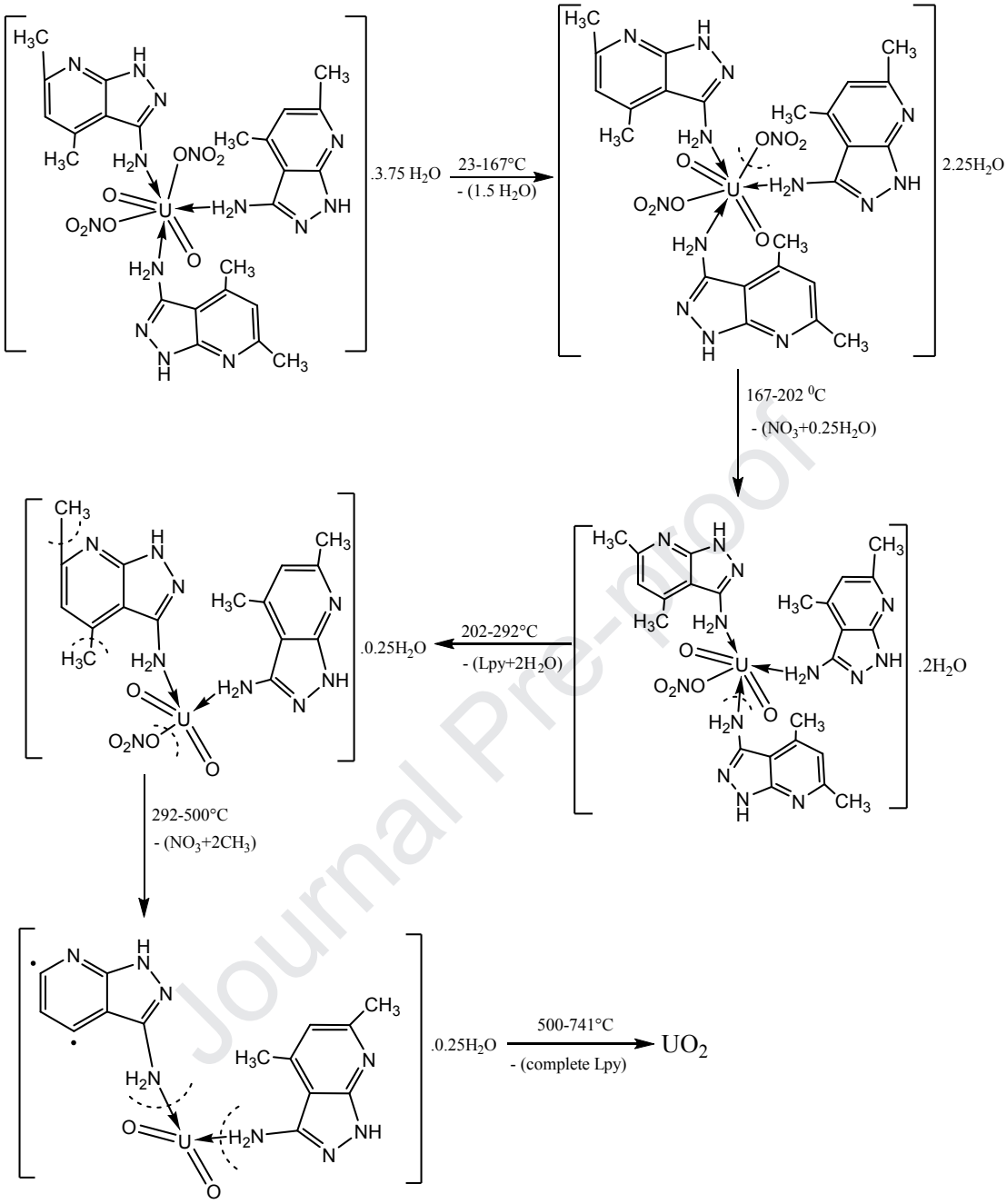

Scheme 6. Thermal decomposition of UO_2(II) complex.

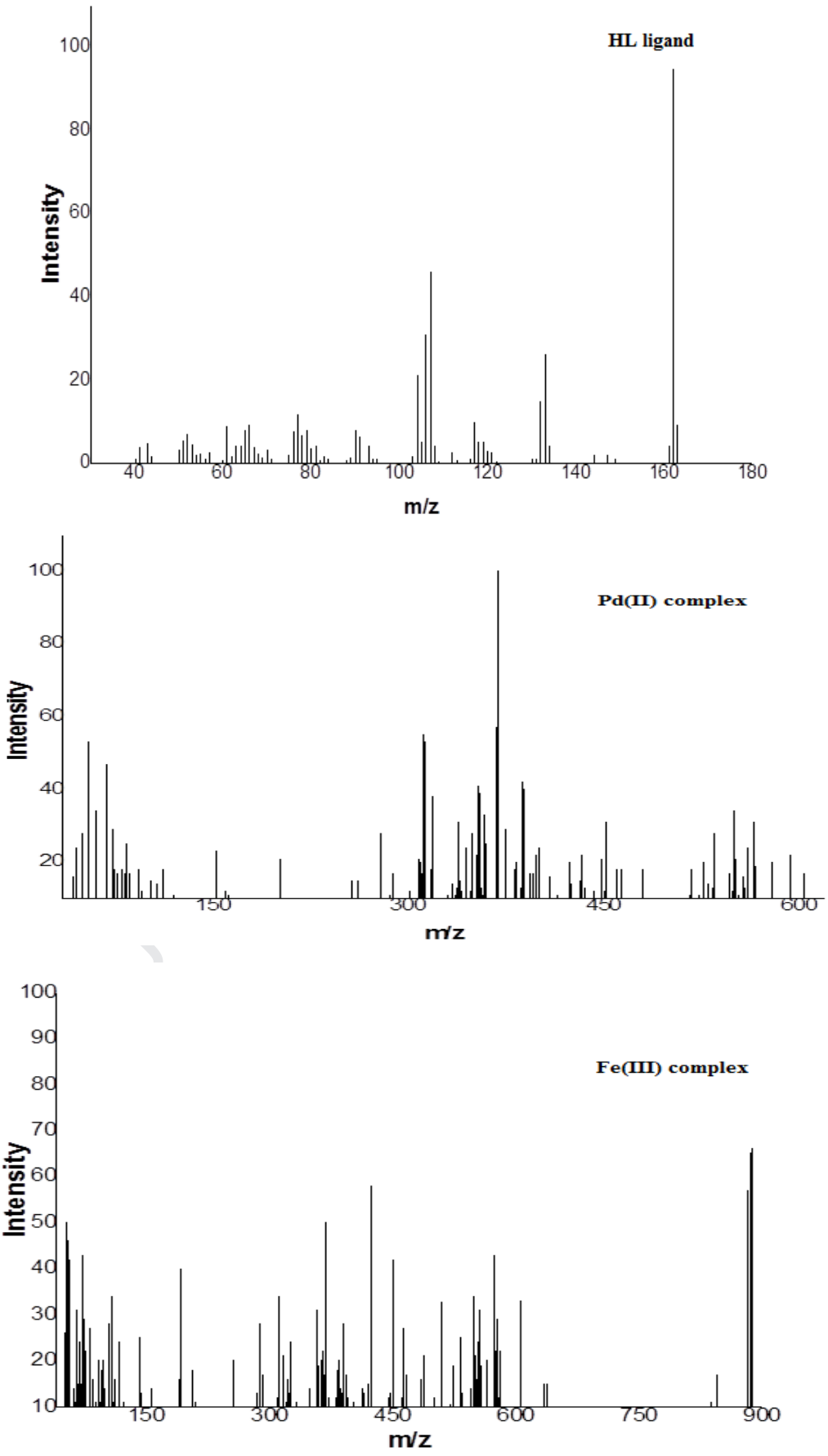

Figure 1. Mass spectra of (HL) ligand and some of its metal complexes

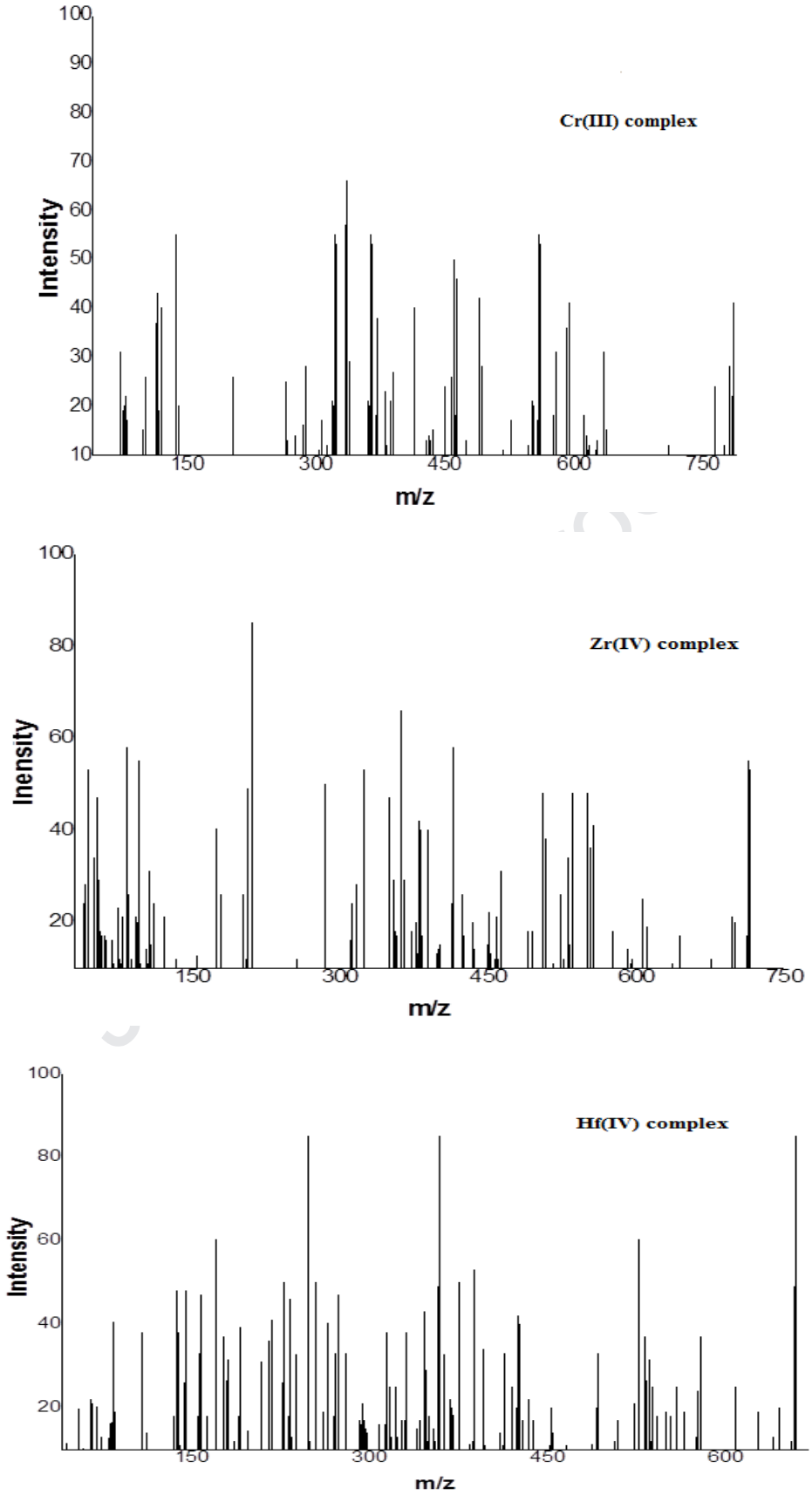

Figure 1. *Continued*

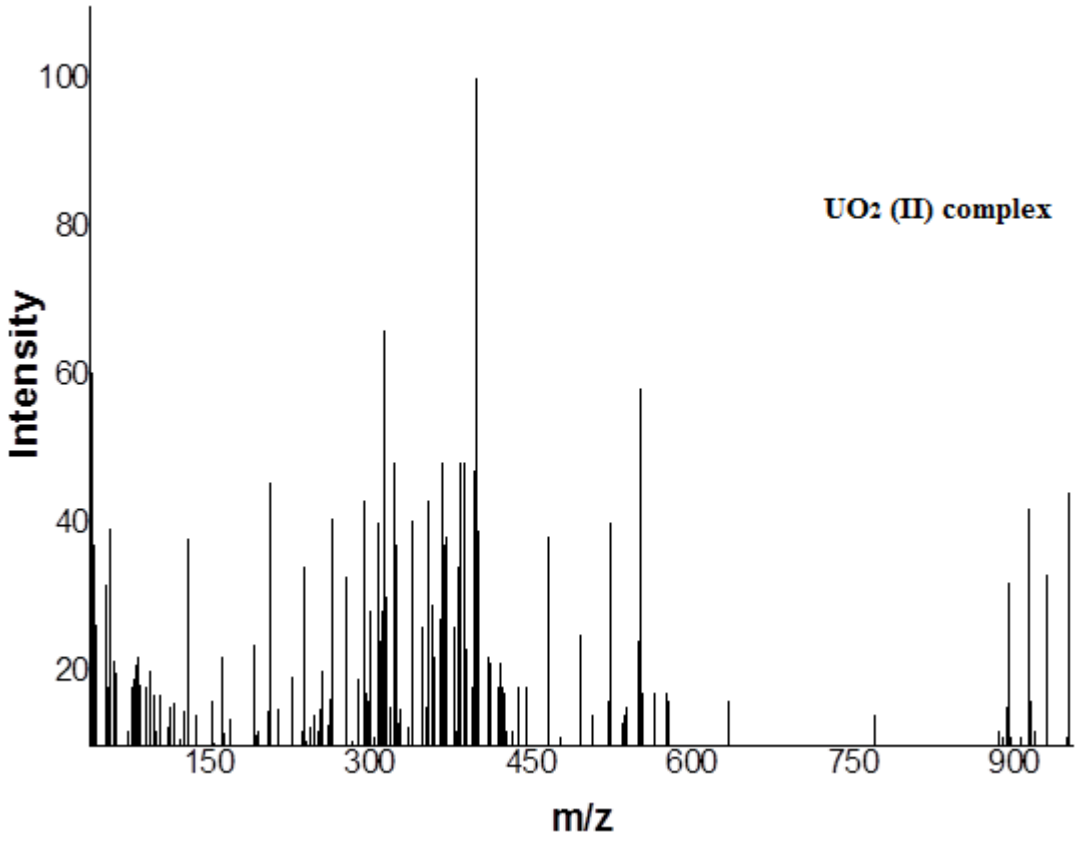

Figure 1. *Continued*

* Mn(II), Pd(II), Fe(III), Cr(III), Ru(III), Hf(IV), Zr(IV) and UO_2(II) metal complexes of 3-amino-4,6- dimethyl-1*H*-pyrazolo[3,4-b]pyridine are prepared .

* The IR suggests that the ligand coordinates to the metal ions as a neutral monodentate moiety .

*All complexes possesses octahedral geometry except the Pd(II) complex.

*Theoretical calculations are performed to corroborate the experimental results.

*Pd(II) complex presents a higher antitumor activity.